Electronic Supplementary Information for

Tuning the Magnetization Dynamics of Tb^{III}-Based Single-Chain Magnets Through Substitution on the Nitronyl Nitroxide Radical

Xiaoqing Liu, Yu-Xia Wang,* Zongsu Han, Tian Han, Wei Shi* and Peng Cheng*

Key Laboratory of Advanced Energy Materials Chemistry (MOE), College of Chemistry, Nankai University, Tianjin 300071, China.

* *To whom correspondence should be addressed. E-mail:* shiwei@nankai.edu.cn; pcheng@nankai.edu.cn; wangyuxiank@163.com

Table of Contents

S1. Plots of Structural Data

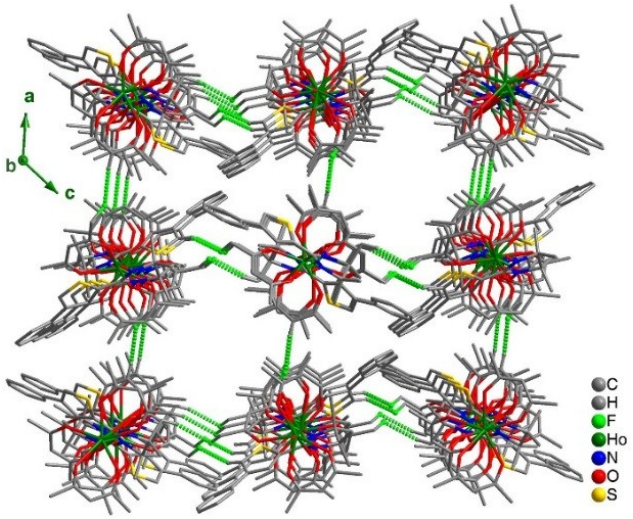

Fig. S1 Packing diagram of **1** along the crystallographic *a* axis with the interchain C−H···F hydrogen bonds.

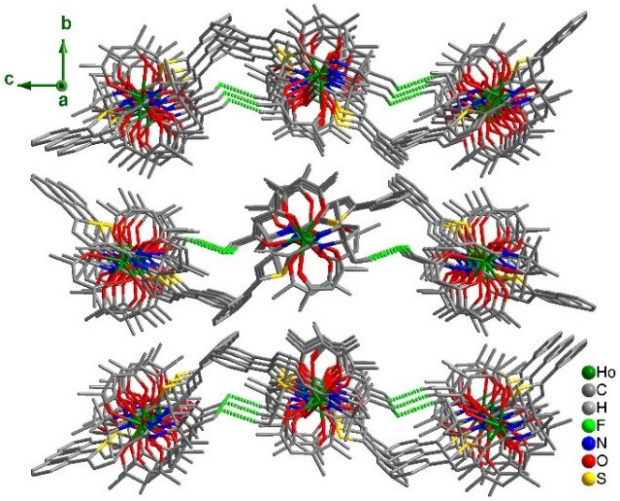

Fig. S2 Packing diagram of **2** along the crystallographic *b* axis with the interchain C−H···F hydrogen bonds.

S2. Magnetic Characterizations

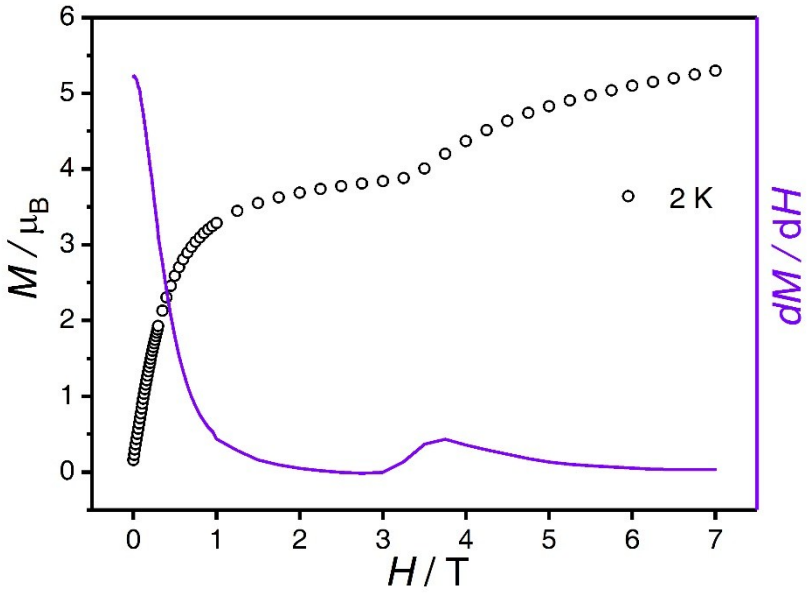

Fig. S3 *M* versus *H* (black circles) and d*M*/d*H* versus *H* (purple solid line) plots for **1** at 2 K.

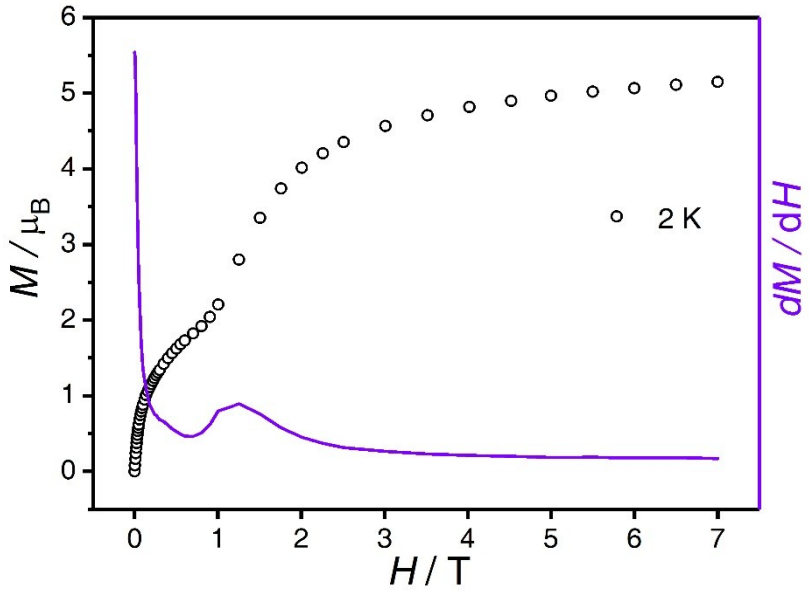

Fig. S4 *M* versus *H* (black circles) and d*M*/d*H* versus *H* (purple solid line) plots for **2** at 2 K.

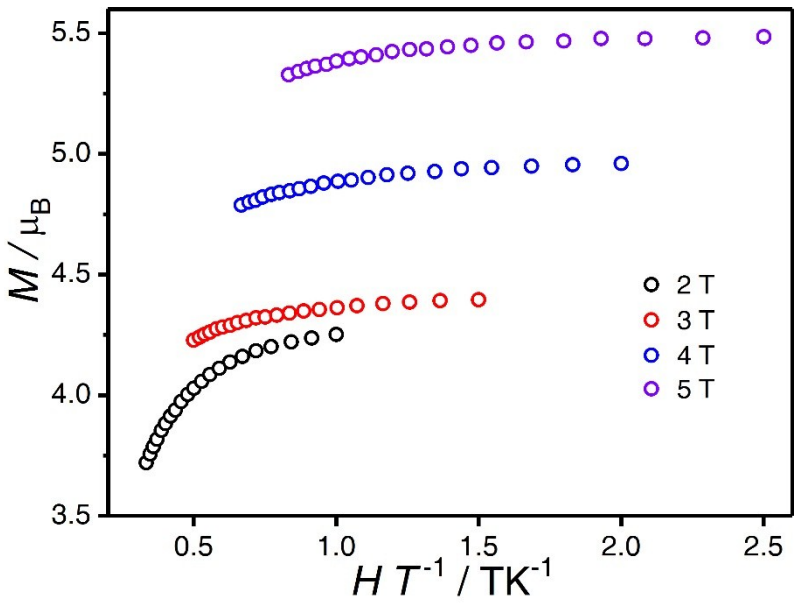

Fig. S5 Magnetization versus HT^{-1} plots obtained at 2, 3, 4 and 5 T for **1**.

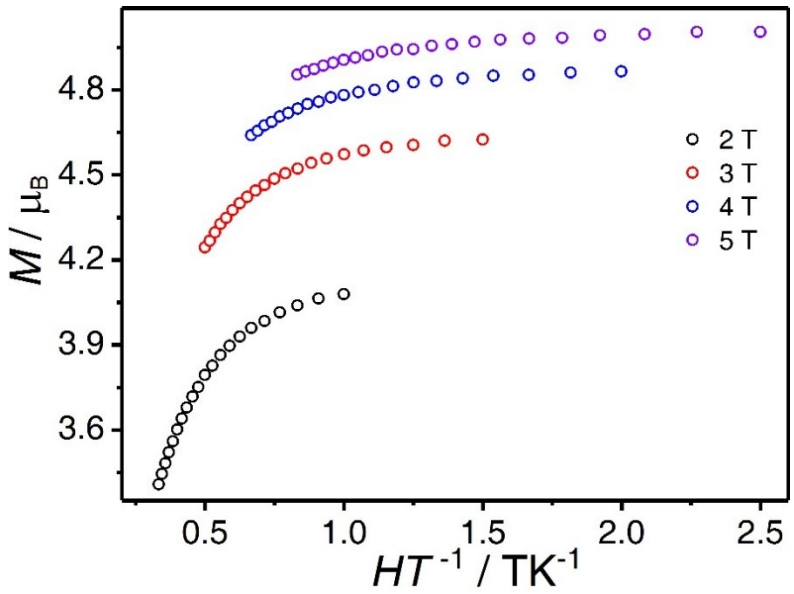

Fig. S6 Magnetization versus HT^{-1} plots obtained at 2, 3, 4 and 5 T for **2**.

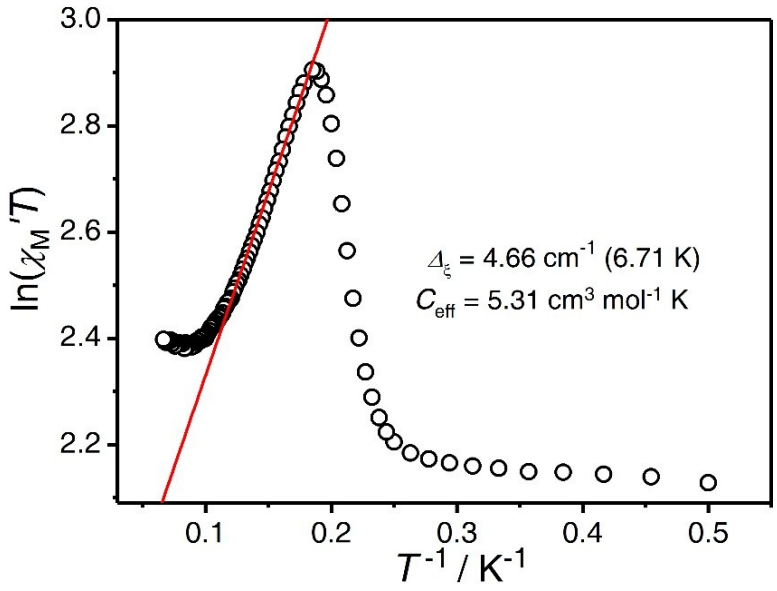

Fig. S7 Plot of $\ln(\chi_M'T)$ versus T^{-1} for **1**. (χ_M' is the real component of variable-temperature a.c. susceptibilities at 1 Hz and zero d.c. field). The solid line corresponds to a linear fit.

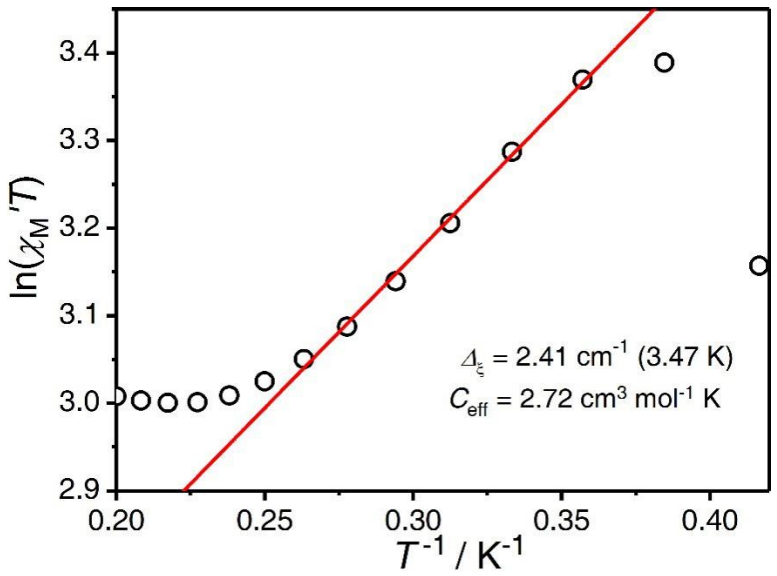

Fig. S8 Plot of $\ln(\chi_M'T)$ *vs.* T^{-1} for **2**. (χ_M' is the real component of variable-temperature a.c. susceptibilities at 1 Hz and zero d.c. field). The solid line corresponds to a linear fit.

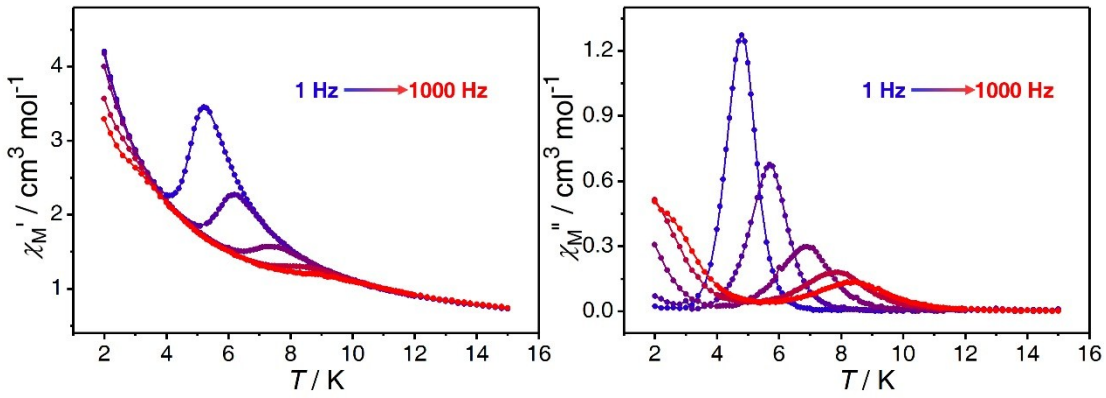

Fig. S9 Variable-temperature a.c. susceptibilities of **1** in the range of 1−1000 Hz under zero applied d.c. field.

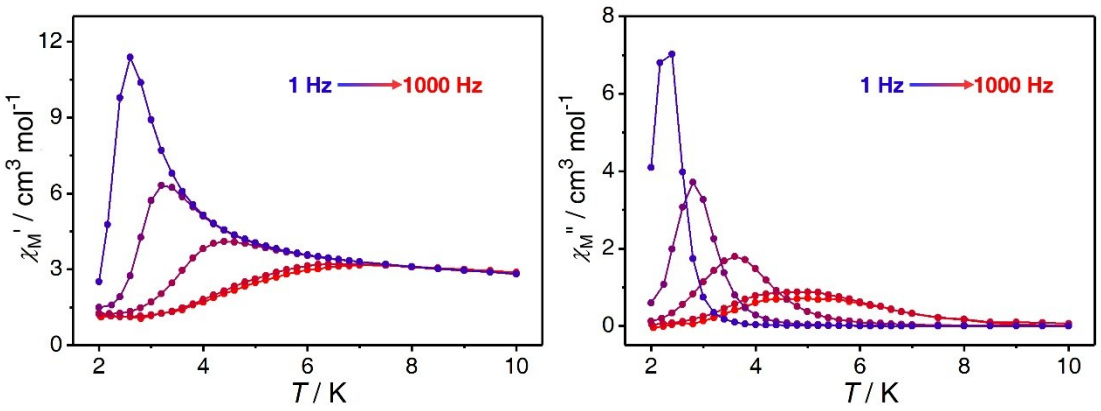

Fig. S10 Variable-temperature a.c. susceptibilities of **2** in the range of 1−1000 Hz under zero applied d.c. field.

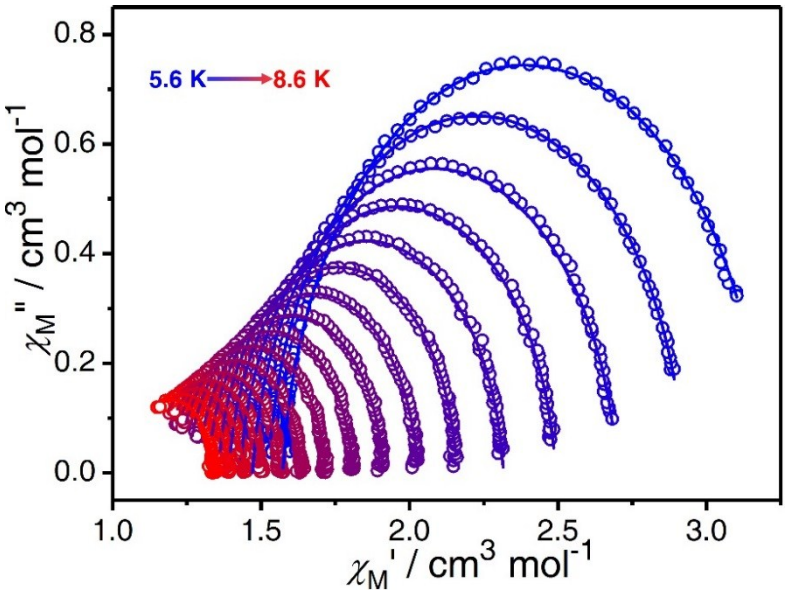

Fig. S11 Cole-Cole plots at zero d.c. field for **1**.

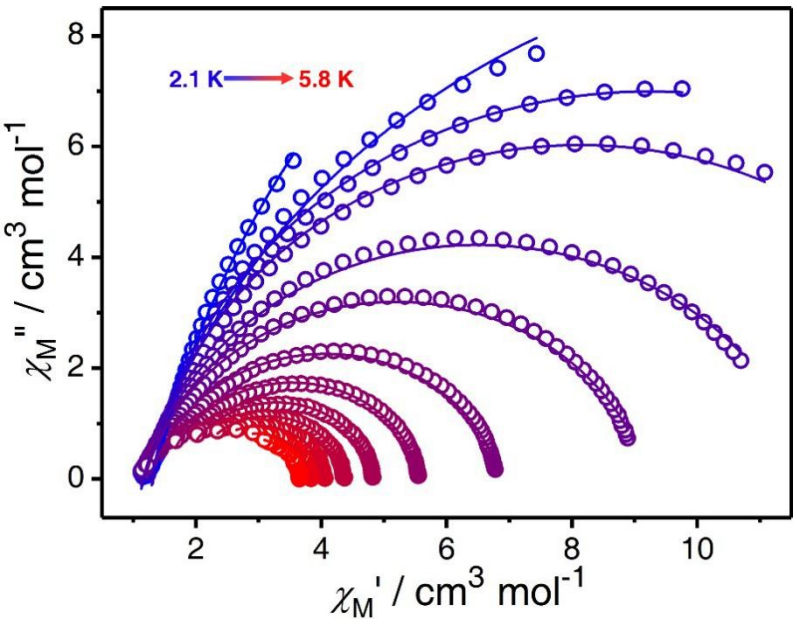

Fig. S12 Cole-Cole plots at zero d.c. field for **2**.

S3. PXRD Patterns

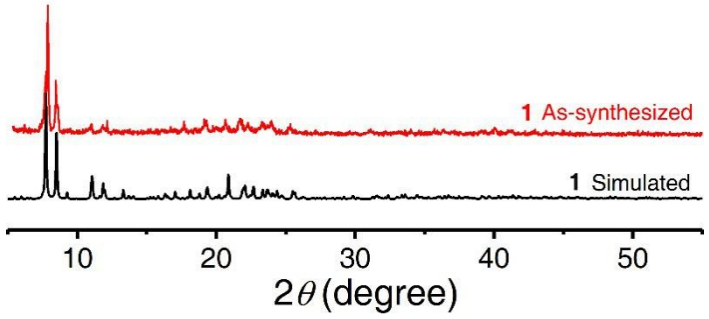

Fig. S13 PXRD pattern of **1** compared with the simulated pattern from the single crystal data of **1**.

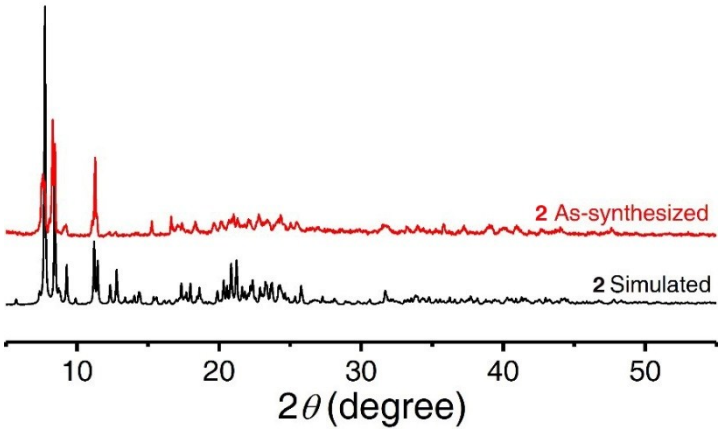

Fig. S14 PXRD pattern of **2** compared with the simulated pattern from the single crystal data of **2**.

S4. Tables

Table S1 Semiquantitative method of polytopal analysis for **1** and **2**[1]

	1-Tb1		**1**-Tb2		DD (D_{2d})	TP (C_{2v})	SAP (D_{4d})
a	O2−O4	2.8419(70)	O9−O11	2.8831(89)	1.199r	1.155r	1.215r
b	O2−O7	3.5778(91)	O9−O15	3.7050(63)	1.499r	1.449r	1.215r
d_1	O4[O2 O7]O5	29.920(19)	O11[O9 O15]O16	23.821(23)	29.5	0.0	0.0
d_2	O3[O1 O6]O8	33.687(22)	O12[O10 O13]O14	30.387(24)	29.5	21.8	0.0
d_3	O4[O1 O7]O8	32.188(24)	O12[O9 O13]O16	32.971(18)	29.5	48.2	52.4
d_4	O3[O2 O6]O5	26.880(22)	O11[O10 O15]O14	27.081(23)	29.5	48.2	52.4
f_1	O3−O4−O6−O7	0.584(16)	O11−O12−O13−O15	1.968(16)	0	14.1	24.5
f_2	O5−O8−O2−O1	2.012(17)	O14−O16−O9−O10	1.008(19)			
	2-Tb1		**2**-Tb2		DD (D_{2d})	TP (C_{2v})	SAP (D_{4d})
a	O1−O3	2.8485(44)	O11−O12	2.8121(41)	1.199r	1.155r	1.215r
b	O1−O5	3.4921(44)	O11−O9	3.4614(38)	1.499r	1.449r	1.215r
d_1	O3[O1 O5]O6	31.932(14)	O12[O11 O9]O14	31.545(13)	29.5	0.0	0.0
d_2	O4[O2 O16]O7	33.989(12)	O13[O15 O8]O10	32.183(11)	29.5	21.8	0.0
d_3	O4[O5 O16]O6	21.508(11)	O13[O15 O9]O14	25.633(11)	29.5	48.2	52.4
d_4	O3[O1 O2]O7	31.718(15)	O12[O11 O8]O10	26.129(12)	29.5	48.2	52.4
f_1	O3−O4−O1−O16	4.162(11)	O12−O13−O11−O15	2.338(85)	0	14.1	24.5
f_2	O6−O7−O2−O5	2.693(10)	O10−O14−O9−O8	2.592(12)			

A[B C]D is the dihedral angle between the ABC plane and the BCD plane. A−B−C−D is the dihedral angle between the (AB)CD and AB(CD) plane, where (AB) signifies the midpoint of the AB edge.

Table S2 Interchain hydrogen bonds (Å) and the angles (°) for **1** and **2**

1	
C5···F32A / H5···F32A / C5–H5–F32A	3.320(7) / 2.425(7) / 161.89(2)
C46···F9 / H46C···F9 / C46–H46C–F9	3.265(8) / 2.422(7) / 146.65(5)
C56···F10 / H56···F10 / C56–H10–F10	3.427(8) / 2.554(1) / 156.79(1)
2	
C33···F2 / H33B···F2 / C33–H33B–F2	3.280(1) / 2.457(9) / 143.66(4)

Table S3 The best results fitted for Cole-Cole plots of **1** by a generalized Debye model

T (K)	χ_S (cm^3 mol^{-1})	χ_T (cm^3 mol^{-1})	τ (s)	α
5.6	1.57296	3.20026	3.04×10^{-2}	0.057
5.8	1.52530	2.92603	1.97×10^{-2}	0.046
6.0	1.47147	2.69931	1.29×10^{-2}	0.064
6.2	1.43045	2.49168	8.76×10^{-3}	0.057
6.4	1.39197	2.31651	5.90×10^{-3}	0.056
6.6	1.35764	2.15914	4.23×10^{-3}	0.042
6.8	1.3224	2.02747	2.91×10^{-3}	0.048
7.0	1.29007	1.91185	2.12×10^{-3}	0.049
7.2	1.25576	1.80821	1.55×10^{-3}	0.042
7.4	1.22401	1.71594	1.13×10^{-3}	0.040
7.6	1.1958	1.63623	8.51×10^{-4}	0.045
7.8	1.16977	1.56410	6.47×10^{-4}	0.047
8.0	1.14109	1.49704	5.11×10^{-4}	0.030
8.2	1.12329	1.43985	3.97×10^{-4}	0.019
8.4	1.09590	1.38663	3.10×10^{-4}	0.011
8.6	1.06363	1.33736	2.57×10^{-4}	0.018

Table S4 The best results fitted for Cole-Cole plots of **2** by a generalized Debye model

T (K)	χ_S (cm^3 mol^{-1})	χ_T (cm^3 mol^{-1})	τ (s)	α
2.5	1.32196	14.94627	8.92×10^{-2}	0.078
2.75	1.15341	11.85144	3.08×10^{-2}	0.149
3.0	1.18549	9.20818	1.28×10^{-2}	0.143
3.4	1.29182	6.84737	4.27×10^{-3}	0.131
3.8	1.50227	5.56876	1.69×10^{-3}	0.099
4.2	1.75601	4.82711	7.78×10^{-4}	0.068
4.6	1.94537	4.35962	4.23×10^{-4}	0.042
5.0	1.99649	4.04789	2.01×10^{-4}	0.045

S5. Crystal Structures and a.c. Magnetic Property of [Tb(hfac)$_3$(NIT-5-ThienPh)$_2$]

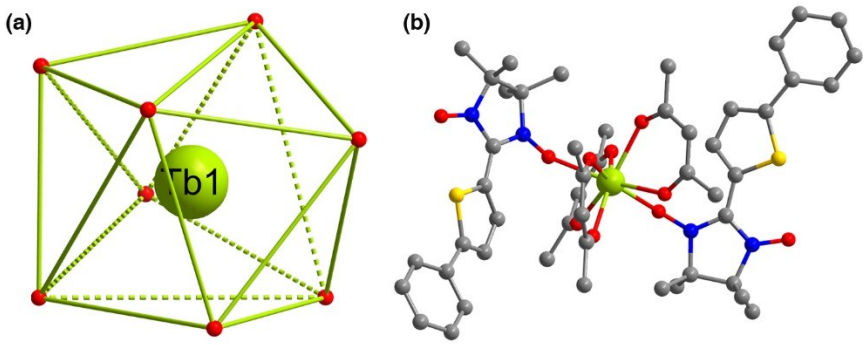

Fig. S15 (a) Coordination polyhedron of the Tb^{III} ion in [Tb(hfac)$_3$(NIT-5-ThienPh)$_2$]. (b) Molecular structure of [Tb(hfac)$_3$(NIT-5-ThienPh)$_2$].

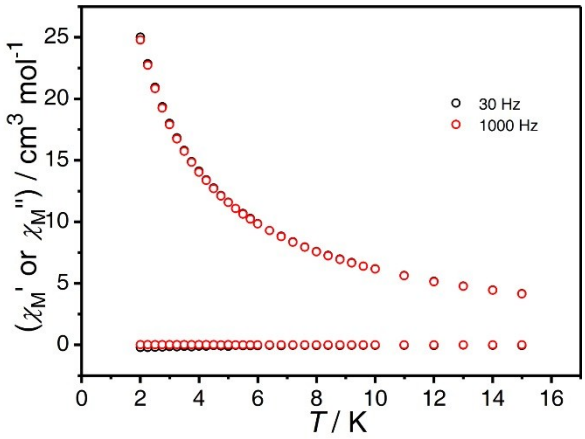

Fig. S16 Variable-temperature a.c. susceptibilities of [Tb(hfac)$_3$(NIT-5-ThienPh)$_2$] under zero applied d.c. field.

S6. References

(1) (a) L. Muetterties and L. J. Guggenberger, *J. Am. Chem. Soc*., 1974, **96**, 1748−1756; (b) M. G. B. Drew, *Coord. Chem. Rev*., 1977, **24**, 179−275.